Chemical Engineering Science 153 (2016) 212–220

Contents lists available at ScienceDirect

Chemical Engineering Science

journal homepage: www.elsevier.com/locate/ces

Extending an equation of state to confined fluids with basis on molecular simulations

Gabriel D. Barbosa [a], Leonardo Travalloni [a,*], Marcelo Castier [b], Frederico W. Tavares [a,c]

[a] Escola de Química, Universidade Federal do Rio de Janeiro, Rio de Janeiro, C.P. 68542, Brazil
[b] Chemical Engineering Program, Texas A&M University at Qatar, P.O. Box 23874, Doha, Qatar
[c] Programa de Engenharia Química – COPPE, Universidade Federal do Rio de Janeiro, Rio de Janeiro, C.P. 68542, Brazil

HIGHLIGHTS

- The Peng–Robinson equation of state was extended to confined fluids.
- The proposed model was based on molecular simulation data.
- Good agreement was obtained with experimental data of mixture adsorption.

ARTICLE INFO

Article history:
Received 30 January 2016
Received in revised form
13 May 2016
Accepted 23 July 2016
Available online 25 July 2016

Keywords:
Peng–Robinson
Adsorption
Monte Carlo
Cylindrical pore

ABSTRACT

The thermodynamic modeling of confined fluids is important to several systems of practical interest. However, the most accurate approaches for describing these systems have a huge computation cost. The development of equations of state is an attractive approach for most chemical engineering common applications. In previous work, the Peng–Robinson equation of state was extended to fluids confined in cylindrical pores, using as starting point the generalized van der Waals theory and proposing purely empirical expressions to model structural properties of the confined fluid. In the present work, the extended Peng–Robinson model was reformulated with basis on molecular simulation data of the confined fluid structure, in substitution to the purely empirical approach. Fluid molecules were considered hard spheres interacting with each other and with the pore wall through square-well potentials. The molecular simulations were performed for several pore sizes, molecule–wall interaction energies, and fluid densities. The obtained equation of state relates the usual thermodynamics properties with the pore size and two molecule–wall interaction parameters for each fluid component. Experimental pure fluid adsorption data were used to estimate the molecule–wall interaction parameters and mixture adsorption predictions were performed without the fitting of binary interaction parameters. Good results were obtained for some systems comprising nanoporous adsorbents, with an improvement over the previous, more empirical approach.

1. Introduction

The thermodynamic description of fluids confined in nanoporous media differs from that of bulk fluids due to the interaction between the fluid molecules and the pore walls. Such effect becomes more pronounced as the confinement dimensions decrease. From a practical point of view, the proper modeling of these systems is important to improve the efficiency of many chemical processes, such as adsorption separations and oil and gas extraction.

Among the alternatives for the modeling of thermodynamic properties of confined fluids, molecular simulations (Alvarez et al., 1999; Frenkel and Smit, 2002) and density functional theory (Peng and Yu, 2008; Wu, 2009) are the most accurate approaches, but have an appreciable computational cost. Thus, the development of models with smaller computational load, which can still provide a satisfactory agreement with experimental data, would be useful for common engineering applications. In this context, an equation of state suitable for fluids under confinement would allow for equilibrium calculations with a small computational effort.

Following this approach, Schoen and Diestler (1998) proposed a modified van der Waals equation of state for Lennard–Jones fluids confined in slit pores, based on perturbation theory. A uniform hard sphere fluid was considered as the reference state and the

* Corresponding author.
E-mail address: travalloni@eq.ufrj.br (L. Travalloni).

http://dx.doi.org/10.1016/j.ces.2016.07.033
0009-2509/

Nomenclature

a	energy parameter of the Peng–Robinson equation of state
a_p	energy parameter modified by confinement
b_1-b_4	functions of pore size in the expression of F_p
b_p	volume parameter modified by confinement
E_{conf}	configurational energy
F_p	fraction of fluid molecules interacting with the pore wall
F_{pp}	value of F_p for packing of the fluid molecules
F_{pr}	value of F_p for random distribution of the fluid molecules
g	function of temperature in the expression of N_c
h	function of pore size in the expression of N_c
k	Boltzmann constant
N	number of fluid molecules
N_{av}	Avogadro number
N_c	molecule–molecule coordination number
NC	number of fluid components
P	pressure
q	internal partition function
Q	canonical partition function
r	distance
R	ideal gas constant
r_p	pore radius
T	temperature
T_c	bulk fluid critical temperature
u	interaction potential
v	molar volume
V	total volume
V_f	free volume
x	mole fraction

Greek letters

α	function of temperature in the energy parameter of the Peng–Robinson equation of state
β	auxiliary term in the model equations
γ	auxiliary term in the model equations
Γ	upper incomplete gamma function
δ	square-well width of the molecule–molecule interaction potential
δ_p	square-well width of the molecule–wall interaction potential
ε	square-well depth of the molecule–molecule interaction potential
ε_p	square-well depth of the molecule–wall interaction potential
ϑ	auxiliary term in the model equations
λ	de Broglie wavelength
μ	chemical potential
ρ	fluid density
ρ_{max}	fluid packing density
σ	molecular diameter
Ω	function of the acentric factor in the Peng–Robinson equation of state

Subscripts

i, j	fluid component

perturbations of the molecule–molecule and molecule–wall interactions were modeled by the mean-field approximation. This model could predict capillary condensation in mesopores. Similarly, Truskett et al. (2001) obtained a model that takes into account the formation of hydrogen bonds in associating confined fluids. Giaya and Thompson (2002) extended this model to cylindrical pores and were able to predict water adsorption experimental data. Using as starting point the thermodynamic theory of interfaces, Zhu et al. (1999) developed an equation of state for Lennard–Jones fluids confined in cylindrical mesopores, which was able to predict the nitrogen adsorption behavior on MCM-41 molecular sieves.

For a confining pore with square cross section, Zarragoicoechea and Kuz (2002) developed a modified van der Waals equation of state, treating the pressure as a tensor and neglecting the molecule–wall interaction. This model showed a good agreement with numerical simulation data of capillary condensation and experimental data of critical temperature shift as a function of the confinement dimension. Dong et al. (2016) used the model expressions for the confined critical point shift proposed by Zarragoicoechea and Kuz (2004) together with a modified Young–Laplace equation, the Peng–Robinson equation of state, and experimental adsorption data, obtaining a good description of hydrocarbon phase equilibria in nanopores.

Holovko and Dong (2009) and Kim et al. (2011) developed equations of state for hard sphere fluids confined in hard, non-attractive pores, obtaining a good agreement with molecular simulation data. Assuming addictive contributions of the molecule–molecule and molecule–wall interactions to the chemical potential, Mohammad et al. (2009) used a simplified local-density approach coupled with the Peng–Robinson equation of state to predict gas adsorption on coal samples, obtaining good results. Similar works are found in the literature (Charoensuppanimit et al., 2015; Yang and Lira, 2012). Tan and Piri (2015) used the perturbed-chain statistical associating fluid theory (PC-SAFT) coupled with the Young–Laplace equation to model the phase equilibrium of fluids confined in cylindrical pores. With this approach, these authors described the phase equilibrium of simple mixtures in mesoporous solids. However, this model includes an additional parameter that must be estimated for each temperature and pore size, limiting its applicability.

In previous work (Travalloni et al., 2010), we extended the van der Waals equation of state to fluids confined in cylindrical pores, using the generalized van der Waals theory as starting point for the explicit modeling of confinement effects. The obtained model was meant to continuously describe the fluid behavior as a function of the confinement degree, with the same set of parameters. This model was able to satisfactorily correlate pure fluid adsorption data and predict the adsorption behavior of some mixtures. Using the same methodology, an extended version of the Peng–Robinson equation of state was also obtained (Travalloni et al., 2014). However, the development of these models was based on a purely empirical modeling of structural properties of the confined fluid.

In the present work, Monte Carlo molecular simulations were performed to evaluate geometric and energetic effects of different confinement degrees on the fluid structure. These data were used to develop analytical expressions for structural properties of the confined fluid, as required by the theoretical approach presented before (Travalloni et al., 2014) for the development of equations of state for confined fluids. In this way, the purely empirical expressions used in previous work to model the confined fluid

structure (Travalloni et al., 2010, 2014) were substituted by simulation-based expressions and an improved version of our extended Peng–Robinson equation of state was proposed.

2. Basic formulation of the equation of state

Here we present a brief of the model formulation, which was detailed elsewhere (Travalloni et al., 2010). From the generalized van der Waals theory (Lee et al., 1985; Sandler, 1985), it is possible to write the canonical partition function as:

$$Q(T, V, N_1, N_2, \ldots N_{NC}) = \prod_{i=1}^{NC} \left(\frac{q_i^{N_i}}{\lambda_i^{3N_i} N_i!} \right) V_f^N \exp\left(\int_\infty^T \frac{E_{conf}}{kT^2} dT \right) \quad (1)$$

where T is the absolute temperature, V is the volume of the system, N is the number of molecules, q is the internal partition function, λ is the de Broglie wavelength, V_f is the free volume, E_{conf} is the configurational energy, k is the Boltzmann constant, NC is the number of fluid components, and subscript i refers to component i. The free volume was modeled in consistency with the Peng–Robinson equation of state combined with the classical mixing rule for the volume parameter:

$$V_f = V - \sum_{i=1}^{NC} \left(\frac{N_i}{\rho_{max,i}} \right) \quad (2)$$

where $\rho_{max,i}$ is the close-packing molecular density of component i. Based on packing data compiled by Mueller (2005), the following expression was fitted to $\rho_{max,i}$ (Travalloni et al., 2010):

$$\rho_{max,i}\sigma_i^3 = c_1 - c_2 \exp\left(c_3 \left(0.5 - \frac{r_p}{\sigma_i} \right) \right) + c_4 \exp\left(c_5 \left(0.5 - \frac{r_p}{\sigma_i} \right) \right) \quad (3)$$

where σ_i is the molecular diameter of component i, r_p is the pore radius, and $c_1 = 1.158$, $c_2 = 0.479$, $c_3 = 0.621$, $c_4 = 0.595$, and $c_5 = 4.014$ are universal parameters (i.e., there is no need to re-estimate these parameters). For consistency with the Peng–Robinson model, σ_i should be calculated from the volume parameter of the equation of state (Travalloni et al., 2014).

Molecule–molecule interactions were assumed to follow the square-well potential:

$$u_{ij}(r_{ij}) = \begin{cases} \infty, & r_{ij} \le \sigma_{ij} \\ -\varepsilon_{ij}, & \sigma_{ij} < r_{ij} \le \sigma_{ij} + \delta_{ij} \\ 0, & r_{ij} > \sigma_{ij} + \delta_{ij} \end{cases} \quad (4)$$

where r_{ij} is the distance between a pair of fluid molecules, σ_{ij} is the mean molecular diameter for these molecules, ε_{ij} is the depth of the square-well, and δ_{ij} is its width. Similarly, the molecule–wall interactions were assumed to follow a square-well potential of the form:

$$u_i(r_i) = \begin{cases} \infty, & r_i \ge r_p - \sigma_i/2 \\ -\varepsilon_{p,i}, & r_p - \sigma_i/2 - \delta_{p,i} \le r_i < r_p - \sigma_i/2 \\ 0, & r_i < r_p - \sigma_i/2 - \delta_{p,i} \end{cases} \quad (5)$$

where r_i is the radial position of a fluid molecule inside the pore, $\varepsilon_{p,i}$ is the depth of the molecule–wall square-well, and $\delta_{p,i}$ is its width. This potential function defines three regions inside the pore, as depicted in Fig. 1, where region I is outside the range of the molecule–wall attraction, region II is within this range, and region III is unavailable to the fluid because of the molecule–wall hardcore repulsion.

Assuming pairwise additivity for the molecule–molecule and molecule–wall interactions, the configurational energy is:

$$E_{conf} = -\frac{1}{2} \sum_{i=1}^{NC} \sum_{j=1}^{NC} \left(N_j N_{c,ij} \varepsilon_{ij} \right) - \sum_{i=1}^{NC} \left(N_i F_{p,i} \varepsilon_{p,i} \right) \quad (6)$$

where $N_{c,ij}$ is the molecule–molecule coordination number and $F_{p,i}$ is the fraction of component i molecules interacting with the pore wall (i.e., the fraction of molecules in region II of Fig. 1). In this work, these structural properties were modeled with basis on molecular simulation data (next section). Estimation of parameters present in the expressions proposed for $N_{c,ij}$ and $F_{p,i}$ was performed through the particle swarm optimization method (Schwaab et al., 2008). With such expressions, the equation of state (explicit in pressure) and the chemical potential of a fluid component were analytically obtained from the partition function (Eq. (1)) by:

$$P = kT \left(\frac{\partial(\ln Q)}{\partial V} \right)_{T,N_1,N_2,\ldots N_{NC}} \quad (7)$$

$$\mu_i = -kT \left(\frac{\partial(\ln Q)}{\partial N_i} \right)_{T,V,N_{j \ne i}} \quad (8)$$

3. Molecular simulation

Grand Canonical Monte Carlo simulations (Frenkel and Smit, 2002) were performed in order to investigate the structural behavior of a pure confined fluid (hence, subscripts that identify fluid components will be dropped in this section). For consistency with the assumptions made in the analytical development of the equation of state, a confining pore was represented by a cylindrical simulation box with periodic boundary condition in the axial coordinate and the fluid molecules were modeled as spheres interacting with each other and with the pore wall through the potential functions in Eqs. (4) and (5), respectively. In the equilibration step, 3×10^8 configurations were generated; sampling and statistics of equilibrium properties were carried out over the last 3×10^8 configurations. Average values of N_c and F_p were obtained for different pore sizes ($r_p/\sigma = 1.5$–20), molecule–wall interaction energies ($\varepsilon_p/\varepsilon = 0$–$15.6$), and fluid densities ($\rho/\rho_{max} \approx 0$–$0.8$, where ρ_{max} was calculated with Eq. (3)). The temperature and the square-well width of each potential function were kept constant ($kT/\varepsilon = 1.97$ and $\delta/\sigma = \delta_p/\sigma = 0.5$). The molecule–molecule coordination number was taken as the number of fluid molecules inside the square-well of a central molecule (i.e., up to a radial distance of 1.5 σ).

Fig. 2 shows profiles of F_p obtained for $r_p/\sigma = 2.5$ and different fluid densities and molecule–wall interaction energies. For high molecule–wall interaction energies ($\varepsilon_p/\varepsilon \ge 7.4$), F_p decreases with increasing density, because the molecule–wall attractive region of the pore (region II in Fig. 1) is preferential to the occupation by fluid molecules, but this region saturates at high densities, so that F_p approaches a packing limit (which depends on the pore size). Due to geometric constraints of the confinement, this limit differs significantly from the value of F_p corresponding to a random distribution of the fluid molecules (dashed line in Fig. 2), which is obtained as the ratio of the volume of region II to the combined volume of regions I and II in Fig. 1:

$$F_{pr} = \frac{(r_p - \sigma/2)^2 - (r_p - \sigma/2 - \delta_p)^2}{(r_p - \sigma/2)^2} \quad (9)$$

On the other hand, for low molecule–wall interaction energies ($\varepsilon_p/\varepsilon \le 1.0$), F_p shows a nonmonotonic behavior as a function of the fluid density, especially for a non-attractive pore wall (Fig. 2). In this case, F_p is close to the random distribution value at low densities and increases to the packing limit at high densities, as

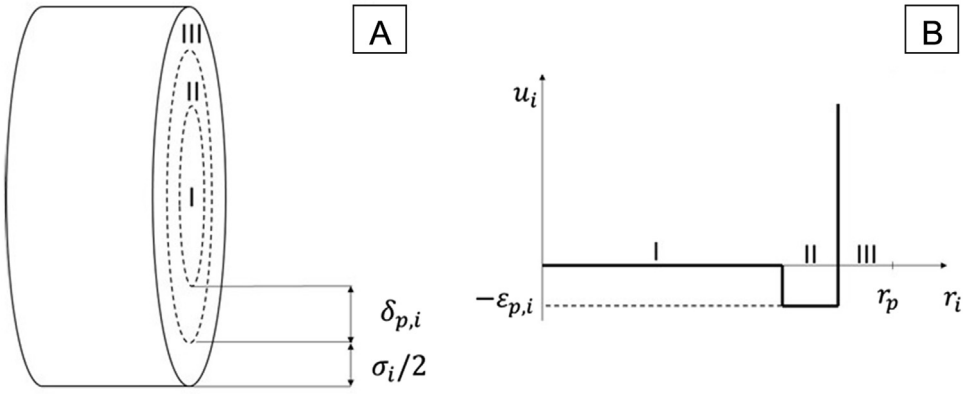

Fig. 1. Regions inside a confining pore (A) as defined by the potential function in Eq. (5) (B).

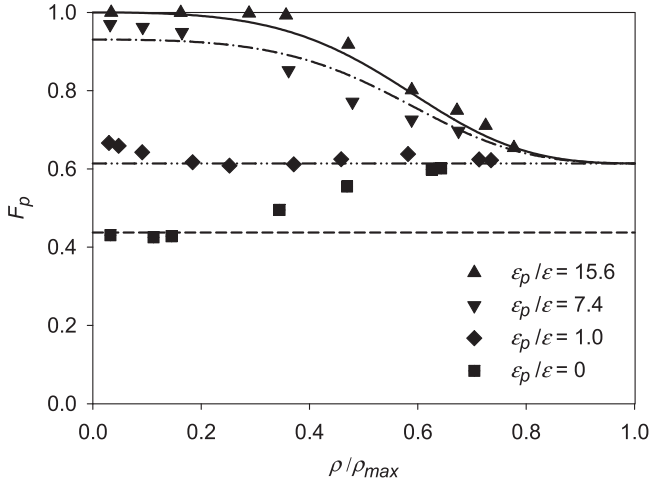

Fig. 2. Simulation data of F_p (symbols) and fitting of Eqs. (10), (11), and (12) (lines) as a function of the fluid density for $r_p/\sigma=2.5$ and different molecule–wall interaction energies ($kT/\varepsilon=1.97$ and $\delta/\sigma=\delta_p/\sigma=0.5$). The dashed line represents the random distribution value of F_p.

Table 1
Universal constants of Eq. (12).

n	C_n
1	12 061.10
2	8682.67
3	1805.26
4	−2.82
5	7.19
6	771.99
7	627.90
8	0.17
9	−0.55
10	88.12
11	455.45
12	−1.88
13	1.63
14	−996.15
15	–1100.87
16	0.44

the geometric constraints become important.

The packing limit of F_p (F_{pp}) approaches the random distribution value when $r_p\to\infty$, because the geometric constraints imposed by the wall become irrelevant. Moreover, $F_{pp}\to 1$ when $r_p\to(\delta_p+\sigma/2)$, i.e., when all the confined molecules are subject to the molecule–wall attraction (see Fig. 1). Thus, the following expression was proposed to model F_{pp}:

$$F_{pp}=F_{pr}+a_1(1-F_{pr})\left(1-\exp\left(-\frac{a_2}{r_p^*}\right)\right) \tag{10}$$

where $r_p^*=r_p/(2\delta_p)$ and $a_1=0.87$ and $a_2=-1.11$ are universal fitting parameters. To model the observed behavior of F_p, the following expression was proposed:

$$F_p=F_{pp}+\frac{(1-F_{pp})\exp\left(-b_1(kT/\varepsilon_p)^{b_2}\right)}{1+b_3\left(\rho/(\rho_{max}-\rho)\right)^{b_4}} \tag{11}$$

where b_k ($k=1$–4) are functions of the pore size, represented by a suitable fitting expression:

$$b_k=C_{4k-3}+\frac{C_{4k-2}}{1+C_{4k-1}\left(r_p^*\right)^{C_{4k}}} \tag{12}$$

and C_n ($n=1$–16) are universal fitting parameters (whose estimated values are presented in Table 1). Eq. (11) satisfies expected physical limits: when $\rho=\rho_{max}$, the packing distribution of the fluid inside the pore is achieved ($F_p=F_{pp}$); when $\rho\to 0$ and $T\to 0$, all the confined molecules occupy the molecule–wall square-well region ($F_p=1$). However, Eq. (11) only represents a monotonic decrease of F_p with increasing fluid density, so that the significantly increasing behavior observed for a non-attractive pore wall (Fig. 2) was not considered in the fitting of Eqs. (10), (11), and (12) to the simulation data. This fitting is illustrated in Figs. 2 and 3 (for two pore sizes), which show a good correlation of the simulation data, even

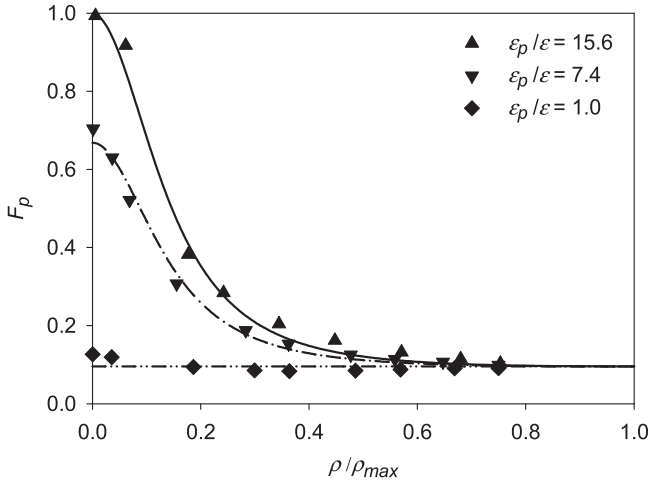

Fig. 3. Simulation data of F_p (symbols) and fitting of Eqs. (10), (11), and (12) (lines) as a function of the fluid density for $r_p/\sigma=20.0$ ($kT/\varepsilon=1.97$ and $\delta/\sigma=\delta_p/\sigma=0.5$).

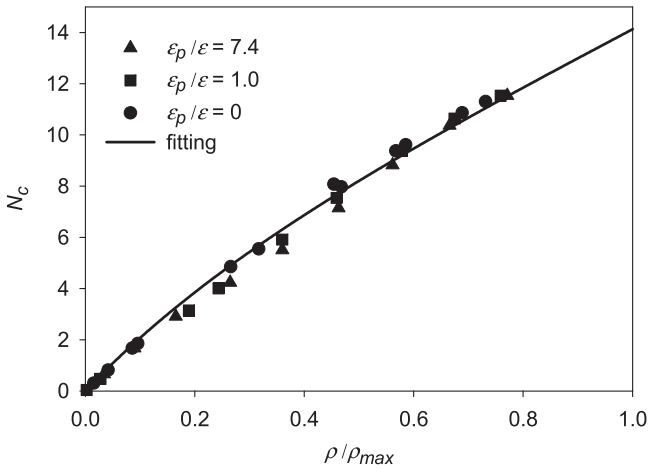

Fig. 4. Simulation data of N_c (symbols) and fitting of Eqs. (15) and (16) (line) as a function of the fluid density for $r_p/\sigma=5.0$ and different molecule–wall interaction energies ($kT/\varepsilon=1.97$ and $\delta/\sigma=\delta_p/\sigma=0.5$).

for profiles with large plateaus at low densities (observed for narrow pores and high molecule–wall interaction energies).

Fig. 4 shows profiles of N_c for $r_p/\sigma=5.0$ and different fluid densities and molecule–wall interaction energies. It is seen that the average value of N_c is little sensitive to the molecule–wall interaction. The geometric effect of confinement on N_c is shown in Fig. 5. This effect is appreciable only for narrow pores. In fact, there is an insignificant difference between the profiles for $r_p/\sigma=10.0$ and 5.0, indicating an approximately bulk behavior of N_c; however, the confinement effect becomes pronounced for $r_p/\sigma=1.5$, reducing the molecule–molecule coordination number due to geometric constrains.

Consistency with the adopted bulk model (the Peng–Robinson equation of state) demands that the expression proposed for the N_c of confined fluids reduces to the expression underlying such bulk model (Sandler, 1990):

$$N_c=g(T)\ln\left(\frac{1+\left(1+\sqrt{2}\right)\rho/\rho_{max}}{1+\left(1-\sqrt{2}\right)\rho/\rho_{max}}\right) \tag{13}$$

where $g(T)$ is a function of temperature inherent to the Peng–Robinson model, related to the temperature dependence of the energy parameter:

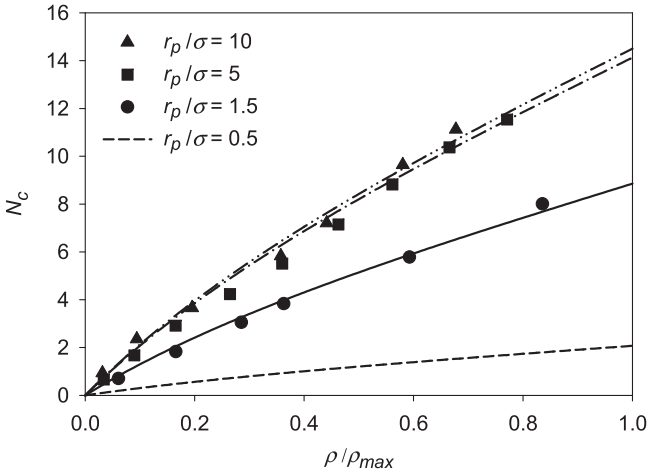

Fig. 5. Simulation data of N_c (symbols) and fitting of Eqs. (15) and (16) (lines) as a function of the fluid density for $\varepsilon_p/\varepsilon=7.4$ and different pore sizes ($kT/\varepsilon=1.97$ and $\delta/\sigma=\delta_p/\sigma=0.5$). The dashed line represents the prediction of these equations for $r_p/\sigma=0.5$.

$$\alpha(T)=\left(1+\Omega\left(1-\sqrt{\frac{T}{T_c}}\right)\right)^2=-T\int_{\infty}^{T}\frac{g(T)}{T^2}dT \tag{14}$$

where T_c is the bulk fluid critical temperature and Ω is a function of the acentric factor. In this sense, the expression proposed for N_c is:

$$N_c=g(T)\ln\left(\frac{1+\left(1+\sqrt{2}\right)\rho/\rho_{max}}{1+\left(1-\sqrt{2}\right)\rho/\rho_{max}}\right)h(r_p/\sigma) \tag{15}$$

where $h(r_p/\sigma)$ is a function that takes into account the effect of the pore size. This function was formulated in consistency with the packing limits of N_c for a bulk fluid ($r_p\to\infty$) and an extremely confined fluid ($r_p/\sigma=0.5$). According to Fig. 5, the profile of N_c for $r_p/\sigma=10.0$ is near the bulk behavior. By fitting Eq. (13) to this profile (i.e., estimating $g(T)$ for the simulated temperature) and extrapolating this equation to $\rho=\rho_{max}$, it was found that the packing limit of N_c for a bulk fluid is about 14, according to the Peng–Robinson model. Regarding an extremely confined fluid, its one-dimensional structure corresponds to a maximum N_c of 2. Therefore, the function $h(r_p/\sigma)$ must reduce the molecule–molecule coordination number by a factor of 7 when $r_p/\sigma=0.5$. In this way, the expression proposed for this function is:

$$h(r_p/\sigma)=1-\frac{6}{7}\exp\left(-m_1\left(\frac{r_p}{\sigma}-0.5\right)^{m_2}\right) \tag{16}$$

where $m_1=0.78$ and $m_2=0.98$ are universal fitting parameters. These parameters were fitted together with the function $g(T)$ corresponding to the simulated temperature. Figs. 4 and 5 show the good performance of Eqs. (15) and (16) in the correlation of the simulation data of N_c. Fig. 5 also includes the prediction of these equations for the one-dimensional, extremely confined fluid ($r_p/\sigma=0.5$), confirming that the corresponding packing limit of N_c is about 2.

4. Equation of state for confined fluids

Eqs. (9–12) were extrapolated to each component of a confined mixture in a straightforward way, giving the model of $F_{p,i}$:

$$F_{pr,i}=\frac{(r_p-\sigma_i/2)^2-(r_p-\sigma_i/2-\delta_{p,i})^2}{(r_p-\sigma_i/2)^2} \tag{17}$$

$$F_{pp,i}=F_{pr,i}+a_1(1-F_{pr,i})\left(1-\exp\left(-\frac{a_2}{r^*_{p,i}}\right)\right) \tag{18}$$

$$b_{k,i}=C_{4k-3}+\frac{C_{4k-2}}{1+C_{4k-1}\left(r^*_{p,i}\right)^{C_{4k}}} \tag{19}$$

$$F_{p,i}=F_{pp,i}+\frac{(1-F_{pp,i})\exp\left(-b_{1,i}\left(kT/\varepsilon_{p,i}\right)^{b_{2,i}}\right)}{1+b_{3,i}\left(x_i\rho/\left(\rho_{max,i}-x_i\rho\right)\right)^{b_{4,i}}} \tag{20}$$

where $r^*_{p,i}=r_p/(2\delta_{p,i})$, x_i is the mole fraction of component i, and constants a_1, a_2, and C_1–C_{16} are the same as for a pure fluid. Regarding the model of $N_{c,ij}$, the expression underlying the Peng–Robinson equation of state for a bulk mixture depends on the adopted mixing rule for the energy parameter. Considering the classical mixing rule, this expression is (Travalloni et al., 2014):

$$N_{c,ij}=g_{ij}(T)\frac{x_i\rho_{max}}{\sqrt{\rho_{max,i}\rho_{max,j}}}\ln\left(\frac{1+\left(1+\sqrt{2}\right)\rho/\rho_{max}}{1+\left(1-\sqrt{2}\right)\rho/\rho_{max}}\right) \tag{21}$$

where ρ_{max} is the packing density of the mixture, which must be consistent with the classical mixing rule for the volume parameter of the equation of state:

$$\rho_{max}=\frac{1}{\sum_{i=1}^{NC}\left(x_i/\rho_{max,i}\right)} \tag{22}$$

For a confined mixture, Eqs. (15) and (16) were extrapolated as:

$$h\left(r_p/\sigma_{ij}\right)=1-\frac{6}{7}\exp\left(-m_1\left(\frac{r_p}{\sigma_{ij}}-0.5\right)^{m_2}\right) \tag{23}$$

$$N_{c,ij}=g_{ij}(T)\frac{x_i\rho_{max}}{\sqrt{\rho_{max,i}\rho_{max,j}}}\ln\left(\frac{1+\left(1+\sqrt{2}\right)\rho/\rho_{max}}{1+\left(1-\sqrt{2}\right)\rho/\rho_{max}}\right)h\left(r_p/\sigma_{ij}\right) \tag{24}$$

where constants m_1 and m_2 are the same as for a pure fluid. With these models of $N_{c,ij}$ and $F_{p,i}$, the equation of state (explicit in pressure) and the chemical potential of a fluid component were obtained from the formulation presented in Section 2:

$$P=\frac{RT}{v-b_p}-\frac{a_p}{v^2+2b_pv-b_p^2}+\frac{RT}{v-b_p}\sum_{i=1}^{NC}\left(\frac{\beta_i\gamma_i\vartheta_i^{b_{4,i}}\left(1-F_{pp,i}\right)}{\left(1+b_{3,i}\vartheta_i^{b_{4,i}}\right)^2}\right) \tag{25}$$

$$\begin{aligned}\mu_i=RT\ln\left(\frac{N_{av}x_i\lambda_i^3}{q_i\left(v-b_p\right)}\right)+\frac{RTb_{p,i}}{v-b_p}-\frac{a_pb_{p,i}v}{b_p\left(v^2+2b_pv-b_p^2\right)}+\frac{\sqrt{2}}{4}\\ \ln\left(\frac{v+\left(1+\sqrt{2}\right)b_p}{v+\left(1-\sqrt{2}\right)b_p}\right)\left(\frac{a_pb_{p,i}}{b_p^2}-\frac{2}{b_p}\sum_{j=1}^{NC}\left(x_ja_{p,ij}\right)\right)-N_{av}\varepsilon_{p,i}F_{pp,i}\\ +\frac{RT\beta_i\gamma_i\left(1-F_{pp,i}\right)}{1+b_{3,i}\vartheta_i^{b_{4,i}}}\left(\frac{\vartheta_i^{b_{4,i}}v}{\left(v-x_ib_{p,i}\right)\left(1+b_{3,i}\vartheta_i^{b_{4,i}}\right)}-\frac{1}{b_{3,i}b_{4,i}}\right)\end{aligned} \tag{26}$$

with:

$$\beta_i=\frac{b_{1,i}^{1/b_{2,i}}b_{3,i}b_{4,i}}{b_{2,i}} \tag{27}$$

$$\gamma_i=\Gamma\left[-1/b_{2,i},\ b_{1,i}\left(RT/N_{av}\varepsilon_{p,i}\right)^{b_{2,i}}\right] \tag{28}$$

$$\vartheta_i=\frac{x_ib_{p,i}}{v-x_ib_{p,i}} \tag{29}$$

$$a_{p,ij}=\sqrt{a_ia_j}\,h\left(r_p/\sigma_{ij}\right) \tag{30}$$

where R is the ideal gas constant, v is the molar volume of the fluid, N_{av} is the Avogadro number, Γ is the upper incomplete gamma function, a_i is the energy parameter of component i in the original (bulk) Peng–Robinson equation of state, which is related to the energy of the molecule–molecule attraction, ε_{ii} (Travalloni et al., 2014), $b_{p,i}$ is the volume parameter of component i modified by the confinement:

$$b_{p,i}=N_{av}/\rho_{max,i} \tag{31}$$

and a_p and b_p are the energy and volume parameters of the mixture, respectively, modified by the confinement:

$$a_p=\sum_{i=1}^{NC}\sum_{j=1}^{NC}\left(x_ix_ja_{p,ij}\right) \tag{32}$$

$$b_p=\sum_{i=1}^{NC}\left(x_ib_{p,i}\right) \tag{33}$$

The resulting model (Eq. (25)) has two terms with the form of the original Peng–Robinson equation of state (except for the modified parameters, a_p and b_p) plus an additional term due to confinement, and has two additional parameters for each component, related to the molecule–wall interactions ($\varepsilon_{p,i}$ and $\delta_{p,i}$), which can be estimated from pure fluid adsorption data. The original Peng–Robinson equation of state is obtained as a particular case of Eq. (25) for $r_p\to\infty$ (i.e., when the confinement effects become negligible).

5. Results of adsorption calculations

To exemplify an application of the equation of state for confined fluids, adsorption equilibrium calculations were carried out according to the methodology described previously (Travalloni et al., 2010). Fig. 6 shows predicted adsorption isotherms of pure ethane for $r_p/\sigma=3.1$, $\varepsilon_p/k=1375.1$, and different values of parameter δ_p. It is noteworthy the versatility of the model in describing different adsorption profiles by varying the molecule–wall interaction parameters (similarly, the shape of the isotherm can be changed by varying the parameter ε_p).

The model was also tested against literature adsorption data with basis on the fitting of the molecule–wall interaction parameters of pure fluids, performed with the particle swarm optimization method (Schwaab et al., 2008). Fig. 7 shows the model fitting to Monte Carlo simulation data (Cao et al., 2004) of pure methane adsorption on MCM-41 molecular sieve (whose pore geometry is remarkably cylindrical and homogeneous) at 207.3 K and a wide pressure range. The obtained parameters are shown in Table 2, together with the average pore radius of the adsorbent. For that temperature, a fair correlation of the simulated data was obtained, yielding an isotherm of type IV in the IUPAC classification (Brunauer et al., 1940), in accordance with a calculation of density functional theory (Cao et al., 2004). Moreover, the model parameters fitted for 207.3 K were used to predict the adsorption behavior of pure methane at higher temperatures, up to 299.0 K

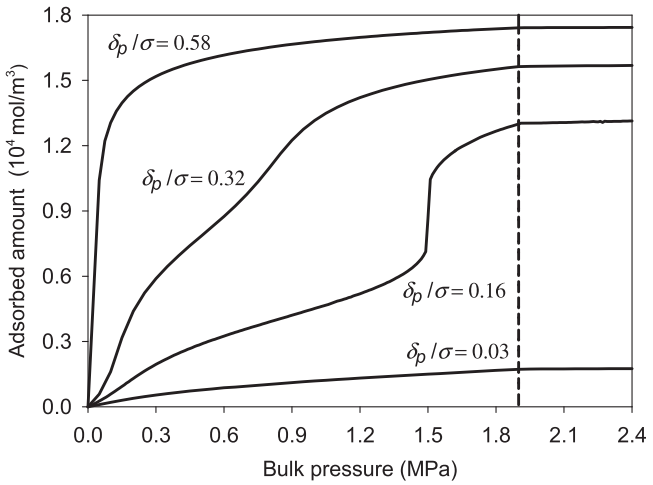

Fig. 6. Pure ethane adsorption at 264 K for $r_p/\sigma=3.10$, $\varepsilon_p/k=1375.10$, and different values of parameter δ_p. Full lines represent the prediction of the model of this work and the dashed line represents the condition of the bulk vapor-liquid transition.

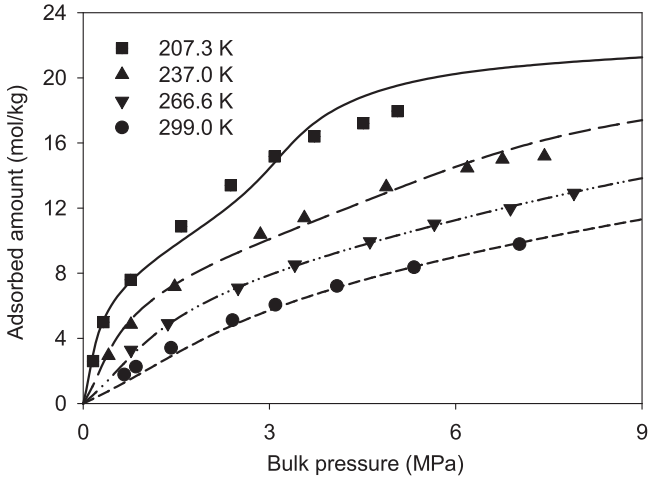

Fig. 7. Pure methane adsorption on MCM-41 at different temperatures. Symbols represent simulation data of Cao et al. (2004) and lines represent the fitting of the model of this work (for the lowest temperature) or model predictions (for the other temperatures).

Table 2
Molecule–wall interaction parameters estimated for pure fluid adsorption.

Reference	Adsorbent	Adsorbate	ε_p/k (K)	δ_p (nm)
Cao et al. (2004)	MCM-41 (r_p=3.14 nm)	methane (σ=0.37 nm)	1147.25	0.12
He and Seaton (2006)	MCM-41 (r_p=1.53 nm)	methane (σ=0.37 nm)	1036.45	0.18
		CO_2 (σ=0.37 nm)	2012.37	0.03
He and Seaton (2003)	MCM-41 (r_p=1.35 nm)	ethane (σ=0.43 nm)	1375.09	0.13
		CO_2 (σ=0.37 nm)	1562.26	0.09
Hefti et al. (2015)	13X (r_p=0.83 nm)	nitrogen (σ=0.36 nm)	1663.25	0.08
		CO_2 (σ=0.37 nm)	2614.87	0.18

(Fig. 7). It is observed that the fitted parameters can be effectively extrapolated over this wide temperature range, which indicates the applicability of the proposed model to temperatures beyond the one which was used for parameter estimation.

Figs 8–10 show the model fitting to experimental adsorption isotherms of pure fluids (methane, ethane, carbon dioxide, and nitrogen) on MCM-41 molecular sieves of smaller pore sizes (He and Seaton, 2003, 2006) or on 13X zeolite (Hefti et al., 2015), whose structure consists of spherical cavities (in this case, an equivalent cylindrical pore radius was calculated from the specific surface area and pore volume reported by Rother and Fieback (2013). The obtained parameters are shown in Table 2. In Figs. 8 and 10, excellent correlations of the experimental data were achieved for those simple isotherms. In Fig. 9A, a good correlation is observed, despite the deviation in the saturation region of the isotherm. This isotherm is clearly of type IV and the model was able to properly represent this nontrivial profile. In Fig. 9B, the isotherm is also of type IV and the model introduced a phase transition at a bulk pressure around 1.4 MPa, resulting in a poorer correlation of the data. However, near this bulk pressure, the experimental isotherm shows a slight increase in slope, possibly due to a capillary condensation.

Using the parameters fitted to pure fluid adsorption data (Table 2), predictions of mixture adsorption were performed with

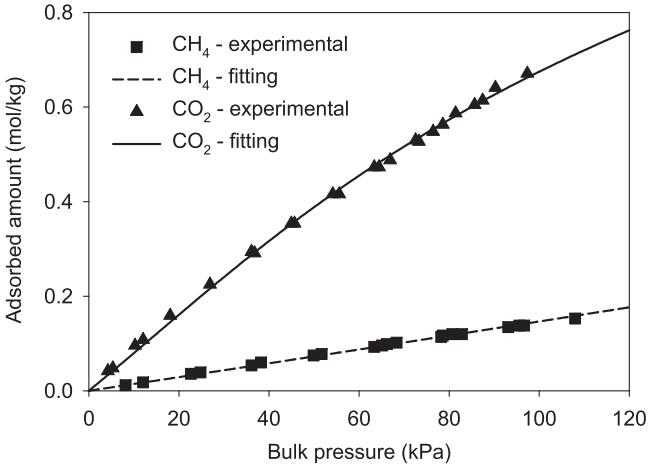

Fig. 8. Pure methane and carbon dioxide adsorption on MCM-41 (r_p=1.53 nm) at 298 K. Experimental data are from He and Seaton (2006) and the fittings are from the model of this work.

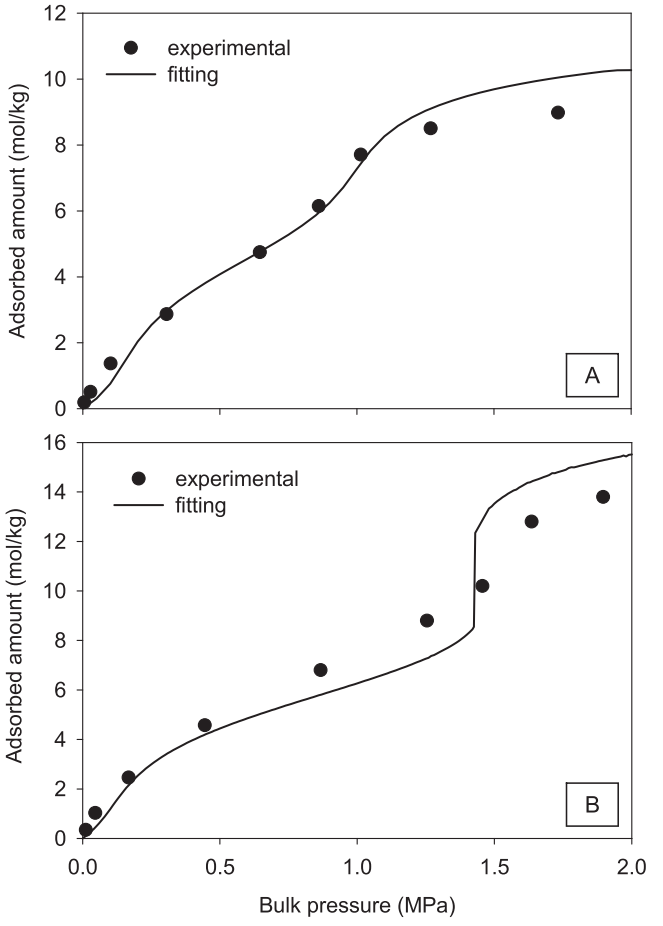

Fig. 9. Pure ethane (A) and carbon dioxide (B) adsorption on MCM-41 (r_p=1.35 nm) at 264.6 K. Experimental data are from He and Seaton (2003) and the fittings are from the model of this work.

the model of this work, with no fitting of binary interaction parameters. These predictions were compared to experimental data (He and Seaton, 2003, 2006; Hefti et al., 2015) for the adsorption of binary mixtures (Figs. 11–14) on the same adsorbents used in the pure fluid adsorption. In Fig. 11, good predictions were obtained for the mixture methane/CO_2 in different bulk pressures and compositions; higher deviations were observed in the adsorbed phase composition, especially at the lowest bulk pressures.

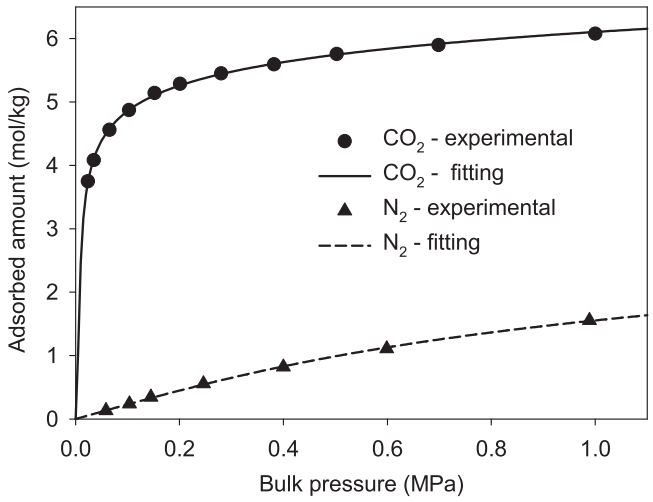

Fig. 10. Pure nitrogen and carbon dioxide adsorption on 13X zeolite (r_p=0.83 nm) at 318 K. Experimental data are from Hefti et al. (2015) and the fittings are from the model of this work.

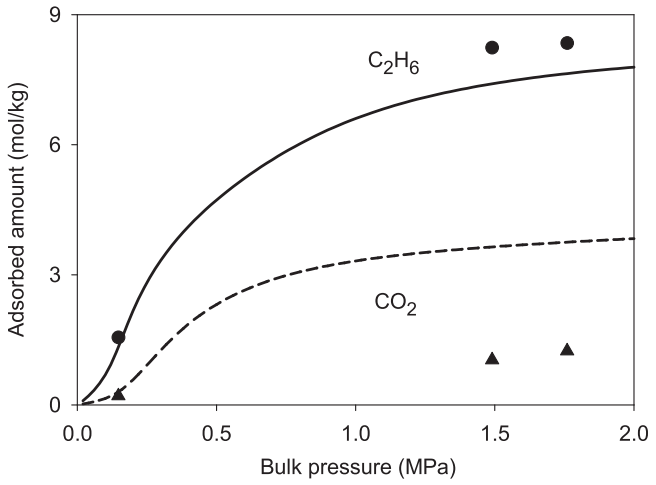

Fig. 12. Binary mixture adsorption on MCM-41 (r_p=1.35 nm) at 264.6 K (bulk mole fractions are 0.8755 for ethane and 0.1245 for carbon dioxide). Symbols represent experimental data of He and Seaton (2003) and lines represent the prediction of the model of this work.

Regarding the mixture ethane/CO_2, predictions are presented for two sets of bulk conditions (Figs. 12 and 13). In the conditions of Fig. 12, it is observed that the model satisfactorily predicted the adsorbed amount of ethane, but overestimated the adsorption of carbon dioxide. It is worth mentioning that the model prediction in Fig. 12 is similar to that provided by the more empirical extension of the Peng–Robinson equation of state to confined fluids, presented in previous work (Travalloni et al., 2014). Fig. 13, on the other hand, displays a scenario of bulk conditions in which the predictive performance of each model is significantly different from one another. In this case, the model of this work showed an improved performance, with a fair prediction of the adsorbed amounts of both components in the mixture, although this model did not provide better correlations of the pure fluids isotherms as compared to the previous modeling. Such improvement in the predictive power of the equation of state is probably due to the modeling of structural properties of the confined fluid with basis on molecular simulation data, instead of a purely empirical modeling.

In Fig. 14, a good prediction is observed for the adsorption of the mixture nitrogen/CO_2, especially for CO_2, even though the

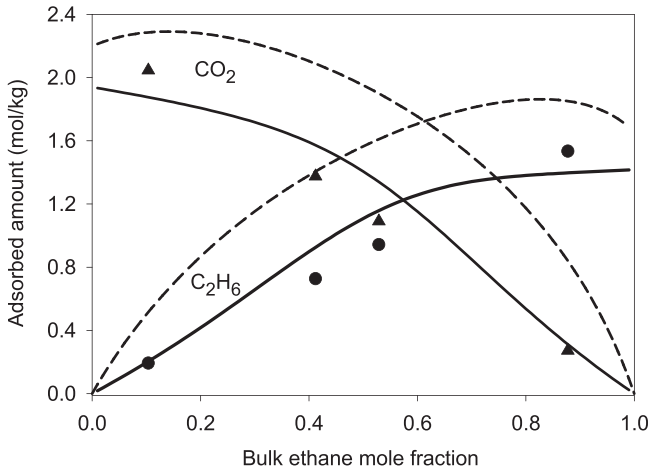

Fig. 13. Binary mixture adsorption on MCM-41 (r_p=1.35 nm) at 264.6 K (bulk pressure is 151.45 kPa). Symbols represent experimental data of He and Seaton (2003), full lines represent the prediction of the model of this work, and dashed lines represent the prediction of the more empirical modeling of Travalloni et al. (2014).

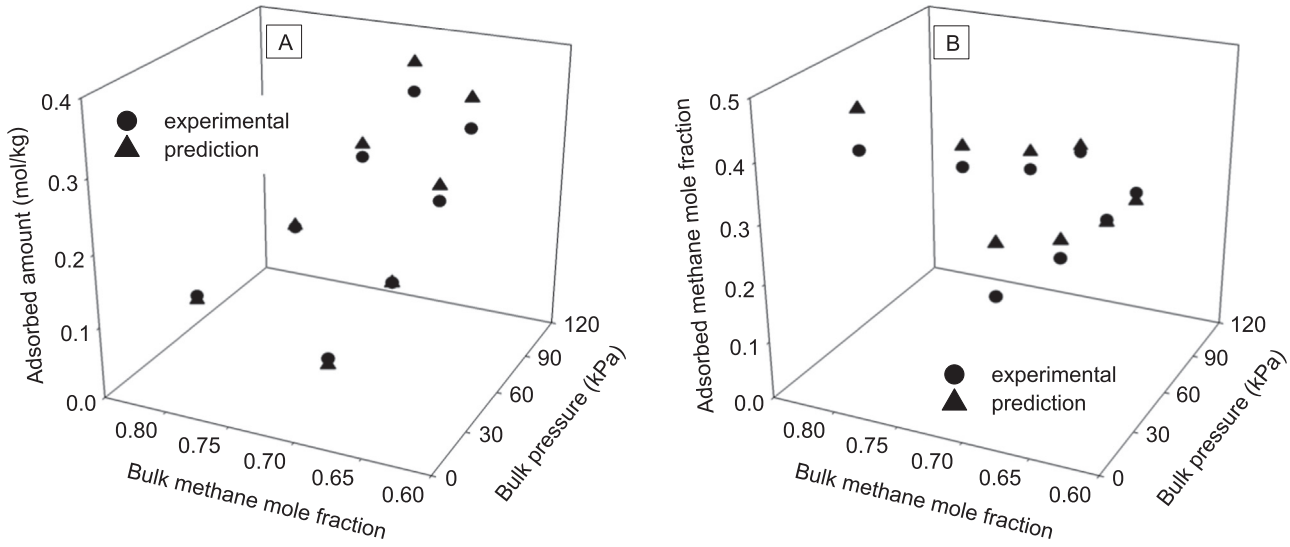

Fig. 11. Methane/CO_2 mixture adsorption on MCM-41 (r_p=1.53 nm) at 298 K: total amount (A) and composition (B) of the adsorbed phase. Experimental data are from He and Seaton (2006) and predictions are from the model of this work.

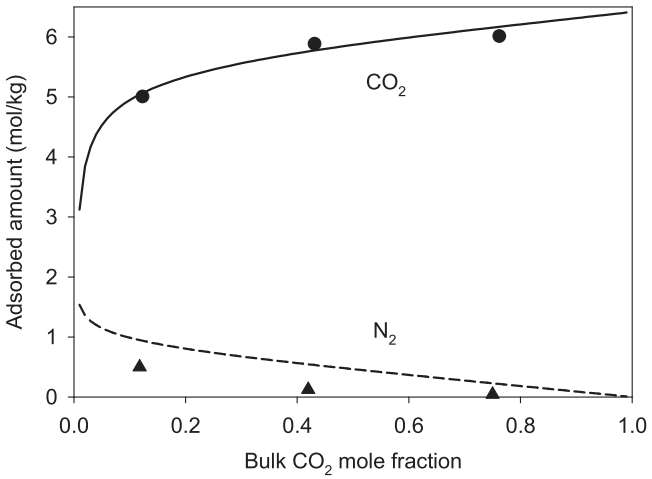

Fig. 14. Binary mixture adsorption on 13X zeolite ($r_p = 0.83$ nm) at 318 K (bulk pressure is 1 MPa). Symbols represent experimental data of Hefti et al. (2015) and lines represent the prediction of the model of this work.

adsorbent (13X zeolite) is characterized by spherical cavities, instead of cylindrical pores. Hefti et al. (2015) predicted the adsorption of this mixture using the ideal adsorbed solution theory (Myers and Prausnitz, 1965), which showed a worse performance for both components. Furthermore, the more empirical model presented in previous work (Travalloni et al., 2014) provided a poor correlation of the pure CO_2 adsorption isotherm, which prejudiced the prediction of the adsorption of this component in the binary mixture.

6. Conclusions

The Peng–Robinson equation of state was extended to fluids confined in cylindrical nanopores, with basis on molecular simulation data of structural properties of the fluid. Analytical expressions containing a set of universal parameters were proposed for these properties. The obtained model relates the properties of the fluid with the confinement dimension and two fitting parameters for each component, allowing for a continuous description of the fluid behavior as a function of the confinement degree. The model showed flexibility in representing different adsorption isotherm profiles. Predictions of the adsorption behavior of binary mixtures showed an improvement over the more empirical approach proposed in previous work, which used expressions with no molecular basis for the confined fluid structural properties. The methodology presented here can be applied to extend other widely used equations of state to confined fluids.

Acknowledgments

This publication was made possible by NPRP Grant # 5-344-2-129 from the Qatar National Research Fund (a member of Qatar Foundation). The statements made herein are solely the responsibility of the authors.

References

Alvarez, M., Levesque, D., Weis, J.J., 1999. Monte Carlo approach to the gas–liquid transition in porous materials. Phys. Rev. E 60, 5495–5504.
Brunauer, S., Deming, L.S., Deming, W.E., Teller, E., 1940. On a theory of the van der Waals adsorption of gases. J. Am. Chem. Soc. 62, 1723–1732.
Cao, D., Shen, Z., Chen, J., Zhang, X., 2004. Experiment, molecular simulation and density functional theory for investigation of fluid confined in MCM-41. Microporous Mesoporous Mater. 67, 159–166.
Charoensuppanimit, P., Mohammad, S.A., Robinson Jr., R.L., Gasem, K.A.M., 2015. Modeling the temperature dependence of supercritical gas adsorption on activated carbons, coals and shales. Int. J. Coal Geol. 138, 113–126.
Dong, X., Liu, H., Hou, J., Wu, K., Chen, Z., 2016. Phase equilibria of confined fluids in nanopores of tight and shale rocks considering the effect of capillary pressure and adsorption film. Ind. Eng. Chem. Res. 55, 798–811.
Frenkel, D., Smit, B., 2002. Understanding Molecular Simulations: from Algorithms to Applications, second ed. Academic Press, San Diego.
Giaya, A., Thompson, R.W., 2002. Water confined in cylindrical micropores. J. Chem. Phys. 117, 3464–3475.
He, Y., Seaton, N.A., 2003. Experimental and computer simulation studies of the adsorption of ethane, carbon dioxide, and their binary mixtures in MCM-41. Langmuir 19, 10132–10138.
He, Y., Seaton, N.A., 2006. Heats of adsorption and adsorption heterogeneity for methane, ethane, and carbon dioxide in MCM-41. Langmuir 22, 1150–1155.
Hefti, M., Dorian, M., Joss, L., Mazzotti, M., 2015. Adsorption equilibrium of binary mixtures of carbon dioxide and nitrogen on zeolites ZSM-5 and 13X. Microporous Mesoporous Mater. 215, 215–228.
Holovko, M., Dong, W., 2009. A highly accurate and analytic equation of state for a hard sphere fluid in random porous media. J. Phys. Chem. B 113, 6360–6365.
Kim, H., Goddard III, W.A., Han, K.H., Kim, C., Lee, E.K., Talkner, P., Hänggi, P., 2011. Thermodynamics of d-dimensional hard sphere fluids confined to micropores. J. Chem. Phys. 134, 114502-1–11.
Lee, K.-H., Lombardo, M., Sandler, S.I., 1985. The generalized van der Waals partition function – II: application to the square-well fluid. Fluid Phase Equilibria 21, 177–196.
Mohammad, S.A., Chen, J.S., Robinson, R.L., Gasem, K.A.M., 2009. Generalized simplified local-density/Peng–Robinson model for adsorption of pure and mixed gases on coals. Energy Fuels 23, 6259–6271.
Mueller, G.E., 2005. Numerically packing spheres in cylinders. Powder Technol. 159, 105–110.
Myers, A.L., Prausnitz, J.M., 1965. Thermodynamics of mixed-gas adsorption. AIChE J. 11, 121–127.
Peng, B., Yu, Y.A., 2008. Density functional theory for Lennard–Jones fluids in cylindrical pores and its applications to adsorption of nitrogen on MCM-41 materials. Langmuir 24, 12431–12439.
Rother, J., Fieback, T., 2013. Multicomponent adsorption measurements on activated carbon, zeolite molecular sieve and metal–organic framework. Adsorption 19, 1065–1074.
Sandler, S.I., 1985. The generalized van der Waals partition function – I: basic theory. Fluid Phase Equilibria 19, 233–257.
Sandler, S.I., 1990. From molecular theory to thermodynamic models – part 1: pure fluids. Chem. Eng. Educ., 12–19.
Schoen, M., Diestler, D.J., 1998. Analytical treatment of a simple fluid adsorbed in a slit-pore. J. Chem. Phys. 109, 5596–5606.
Schwaab, M., Biscaia, E.C., Monteiro, J.L., Pinto, J.C., 2008. Nonlinear parameter estimation through particle swarm optimization. Chem. Eng. Sci. 63, 1542–1552.
Tan, S.P., Piri, M., 2015. Equation-of-state modeling of confined-fluid phase equilibria in nanopores. Fluid Phase Equilibria 393, 48–63.
Travalloni, L., Castier, M., Tavares, F.W., Sandler, S.I., 2010. Thermodynamic modeling of confined fluids using an extension of the generalized van der Waals theory. Chem. Eng. Sci. 65, 3088–3099.
Travalloni, L., Castier, M., Tavares, F.W., 2014. Phase equilibrium of fluids confined in porous media from an extended Peng–Robinson equation of state. Fluid Phase Equilibria 362, 335–341.
Truskett, T.M., Debenedetti, P.G., Torquato, S., 2001. Thermodynamic implications of confinement for a waterlike fluid. J. Chem. Phys. 114, 2401–2418.
Wu, J., 2009. Density functional theory for liquid structure and thermodynamics. In: Lu, X., Hu, Y. (Eds.), Molecular Thermodynamics of Complex Systems. Springer, Berlin.
Yang, X., Lira, C.T., 2012. Modeling of adsorption on porous activated carbons using SLD-ESD model with a pore size distribution. Chem. Eng. J. 195–196, 314–322.
Zarragoicoechea, G.J., Kuz, V.A., 2002. Van der Waals equation of state for a fluid in a nanopore. Phys. Rev. E 65, 021110-1-4.
Zarragoicoechea, G.J., Kuz, V.A., 2004. Critical shift of a confined fluid in a nanopore. Fluid Phase Equilibria 220, 7–9.
Zhu, H.Y., Ni, L.A., Lu, G.Q., 1999. A pore-size-dependent equation of state for multilayer adsorption in cylindrical mesopores. Langmuir 15, 3632–3641.